AGU PUBLICATIONS

JGR

Journal of Geophysical Research: Oceans

RESEARCH ARTICLE

10.1002/2016JC011719

Key Points:
- Analysis of the 2009 non-ENSO like cold event in the Atlantic using in situ data in combination with satellite and reanalysis products
- Results confirm contribution of planetary wave reflection to the 2009 cold event, suggesting the importance of higher baroclinic mode waves
- Indications of an asymmetry in the importance of meridional advection in non-ENSO like cold and warm events

Supporting Information:
- Supporting Information S1

Correspondence to:
K. Burmeister,
kburmeister@geomar.de

Citation:
Burmeister, K., P. Brandt, and J. F. Lübbecke (2016), Revisiting the cause of the eastern equatorial Atlantic cold event in 2009, *J. Geophys. Res. Oceans*, *121*, doi:10.1002/2016JC011719.

Received 11 FEB 2016
Accepted 9 JUN 2016
Accepted article online 13 JUN 2016

Revisiting the cause of the eastern equatorial Atlantic cold event in 2009

Kristin Burmeister[1], Peter Brandt[1,2], and Joke F. Lübbecke[1,2]

[1]GEOMAR Helmholtz Centre for Ocean Research Kiel, Kiel, Germany, [2]Christian-Albrechts-Universität zu Kiel, Kiel, Germany

Abstract An extreme cold sea surface temperature event occurred in the Atlantic cold tongue region in boreal summer 2009. It was preceded by a strong negative Atlantic meridional mode event associated with north-westerly wind anomalies along the equator from March to May. Although classical equatorial wave dynamics suggest that westerly wind anomalies should be followed by a warming in the eastern equatorial Atlantic, an abrupt cooling took place. In the literature two mechanisms—meridional advection of subsurface temperature anomalies and planetary wave reflection—are discussed as potential causes of such an event. Here, for the first time we use in situ measurements in addition to satellite and reanalysis products to investigate the contribution of both mechanisms to the 2009 cold event. Our results suggest that meridional advection is less important in cold events than in corresponding warm events, and, in particular, did not cause the 2009 cold event. Argo float data confirm previous findings that planetary wave reflection contributed to the onset of the 2009 cold event. Additionally, our analysis suggests that higher baroclinic modes were involved.

1. Introduction

2009 was an extreme year for the Tropical Atlantic (TA) [*Foltz and McPhaden*, 2010a]. In January and February, cold Sea Surface Temperature (SST) anomalies developed in the northern TA (12°N–25°N). Associated with stronger than normal north-east trade winds, they triggered a strong negative Atlantic Meridional Mode (AMM) event with anomalously cold Sea Surface Temperatures (SSTs) in the Northern Equatorial Atlantic (NEA) (2°N–12°N) and anomalously warm SSTs along the equator (5°S–2°N) [*Foltz and McPhaden*, 2010a; *Foltz et al*., 2012]. The temperature gradient, that reached its peak in May, was associated with strong north-westerly wind anomalies in the Equatorial Atlantic (EA) consistent with the wind-evaporation-SST feedback [*Carton et al*., 1996; *Chang et al*., 1997] (Figure 1a). These wind anomalies drove anomalous upwelling between 0°N and 6°N and enhanced the cooling in the central basin north of the equator during March–April 2009 [*Foltz et al*., 2012]. The resulting inter-hemispheric SST gradient across the Atlantic equator was the strongest within the last 30 years [*Foltz and McPhaden*, 2010a].

According to classical equatorial wave dynamics, the westerly wind anomalies along the equator during boreal spring should be associated with an anomalously weak Equatorial Undercurrent (EUC) [*Brandt et al*., 2014], a weak eastward shoaling of the equatorial thermocline and an anomalously warm Atlantic Cold Tongue (ACT) during boreal summer [*Philander*, 1986; *Zebiak*, 1993; *Keenlyside and Latif*, 2007]. Such warm events are referred to as canonical events by *Richter et al*. [2013].

In 2009, however, an abrupt cooling of SST took place in the ACT region between May and August 2009, resulting in a strong cold eastern equatorial Atlantic event [*Foltz and McPhaden*, 2010a] (Figure 1b). This cold event was associated with an anomalously weak EUC across most of the basin and thus reduced supply of the equatorial upwelling, typical for canonical warm events [*Brandt et al*., 2014; *Johns et al*.,]. The temperature drop in the ACT region from the warmest ATL3 (20°W–0°E and 3°S–3°N) SSTs during April–May 2009 to the coldest ATL3 SSTs on record in August 2009 is unprecedented since satellite SST measurements started in 1982 [*Foltz and McPhaden*, 2010a; *Brandt et al*., 2014] (Figure 1c).

Analyzing Sea Level Anomaly (SLA) data, *Foltz and McPhaden* [2010b] found that the anomalous northwesterlies in the EA in boreal spring 2009 forced upwelling Rossby waves. *Foltz and McPhaden* [2010a] suggested that the Rossby waves traveled westward during boreal spring and reflected at the western boundary into upwelling equatorial Kelvin waves that propagated eastward and cooled SSTs along the equator

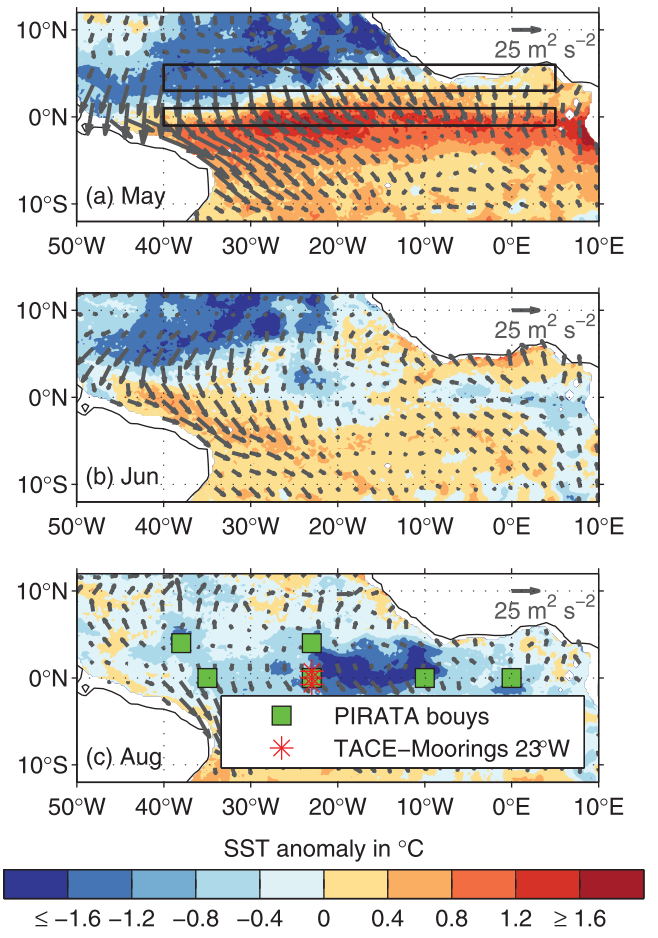

Figure 1. Anomalies of TMI SST (shading) and CCMP pseudo wind stress (arrows) with respect to the climatology mean (1998–2011) for (a) May, (b) June, and (c) August 2009. The black boxes in Figure 1a mark the two latitude bands used in Figure 6, the green squares in Figure 1c marked the positions of PIRATA buoys and the red stars in Figure 1c the positions of TACE moorings.

during boreal summer. They supported their hypothesis with the results of a continuously stratified linear wave model that resolves the first 10 baroclinic modes and 15 meridional modes (Kelvin and the first fourteen Rossby). While the forced Rossby waves can be seen as a strong signal in the observational and model SLA data, the reflected Kelvin wave signal is notably weaker in the observational SLA data and hardly visible in the model output. The importance of Kelvin wave propagation for the development of the 2009 cold event is thus not completely clear yet.

Richter et al. [2013] offered an alternative explanation for what they referred to as noncanonical events, i.e., eastern equatorial Atlantic warm (cold) events that are—in contrast to canonical events—associated with stronger (weaker) trade winds in the western equatorial Atlantic, such as in 2009. They investigated warm events taking place in the ACT region in boreal summer that were preceded by warm SST anomalies in the northern Tropical Atlantic (TA) and an associated weakening of the north-easterly trade winds during boreal spring. The wind change in the northern TA causes a positive subsurface temperature anomaly along ~4°N via Ekman pumping. *Richter et al.* [2013] suggested that this subsurface temperature anomaly is then directly advected into the ACT region by the prevailing equatorward meridional currents leading to positive SST anomalies along the equator. They did not find indications of Rossby wave reflection in the onset of the noncanonical warm events.

The meridional flow in this region is governed by the northern Tropical Cells (TCs) [e.g., *McCreary and Lu*, 1994; *Molinari et al.*, 2003; *Perez et al.*, 2014]. The TCs are shallow overturning circulation cells within the upper 100 m. They are characterized by wind-driven equatorial upwelling, poleward surface Ekman flow, downwelling at about 3–5°N and S, and equatorward geostrophic subsurface flow [e.g., *Lu et al.*, 1998; *Molinari et al.*, 2003; *Perez et al.*, 2014]. *Perez et al.* [2014] found that velocities are higher in the northern TC than in the southern TC and that the northern cell is shifted southward crossing the equator. Their results indicate that the poleward surface flow of the TCs at 23°W intensifies during December–May while the equatorward subsurface flow is strongest during June–November. In 2009, cold subsurface temperature anomalies developed just north of the equator during boreal spring [*Foltz and McPhaden*, 2010a]. While *Richter et al.* [2013] did not specifically address equatorial Atlantic cold events, the meridional advection of those cold subsurface temperature anomalies by the equatorward flow of the northern TC could have contributed to the anomalous cooling of the ACT in summer 2009 [*Perez et al.*, 2014].

In summary, the mechanisms that led to the abrupt cooling in the EA in boreal summer 2009 are still under debate. Meridional advection of subsurface temperature anomalies as well as planetary wave reflection may have been important drivers for it [*Foltz and McPhaden*, 2010a; *Lübbecke and McPhaden*, 2012; *Richter*

Table 1. Deployment Periods and Temporal Data Gaps of PIRATA Temperature Time Series in the Tropical Atlantic

Longitude	Latitude	Period	Data Gaps
38°W	4°N	Mar 1999 to Sep 2013	Jul 1999 to Mar 2000
35°W	0°N	Feb 1998 to Feb 2014	Mar to Sep 2006
23°W	4°N	Jun 2006 to Feb 2014	
23°W	0°N	Mar 1999 to Feb 2014	
10°W	0°N	Sep 1997 to Feb 2014	Nov 1997 to Jan 1999; Jan to Oct 2001; Feb to Dec 2002; Jun 2004 to Jun 2005; Feb to May 2006
0°W	0°N	Feb 1998 to Feb 2014	Jan 1999 to Aug 2000; Feb to Dec 2002; Jun 2004 to May 2005; Jun 2008; May to Sep 2010

et al., 2013; *Perez et al*., 2014]. This study aims to improve the understanding of the development of the 2009 cold event. Therefore, we analyzed in situ subsurface data for the first time in addition to satellite and reanalysis products to clarify the role of both mechanisms in this cold event.

The paper is organized as follows: The data sets and methods are described in section 2. The results are presented in section 3, and section 4 contains a discussion and summary of the cold event in the EA in 2009.

2. Data and Methods

For the analysis, satellite data, reanalysis products, and in situ data sets are used.

Altimetric delayed-time SLAs were produced by Ssalto/DUACS (Developing Use of Altimetry for Climate Studies) and distributed by Archiving, Validation and Interpretation of Satellite Oceanographic Data (AVISO), with support from CNES (Centre National d′ Etudes Spatiales) (http://www.aviso.altimetry.fr/duacs/). AVISO SLAs are calculated by subtracting the reference mean field for the time period 1993 to 1999 from the instantaneous SSH field [*Dibarboure et al*., 2011]. In this study, daily SLA data at a spatial resolution of 0.25° ×0.25° are used for the time period 1993–2012.

Three-day average Remote Sensing Systems Tropical Rainfall Measuring Mission's (TRMM) Microwave Imager (TMI) SST data from 1998 to 2014 are used (www.remss.com/missions/tmi). The data set has a spatial resolution of 0.25°×0.25°.

Pseudo wind stress and wind velocity components are available from the Physical Oceanography Distributed Active Archive Center (PODAAC) as part of the gridded five-daily and monthly Cross-Calibrated Multi-Platform (CCMP) Ocean Surface Wind Components [*Atlas et al*., 2011]. The data set covers a period from July 1987 to 2011 and has a spatial resolution of 0.25°×0.25°.

Monthly ocean temperature, salinity, and velocity fields from 1980 to 2014 are produced by NCEP Global Ocean Data Assimilation System (GODAS) at the National Environmental Prediction Center (NCEP) [*Behringer and Xue*, 2004]. Temperature and salinity profiles are assimilated in a 3DVAR scheme designed by *Derber and Rosati* [1989]. The model has 40 vertical levels and is forced by the momentum flux, heat flux, and fresh water flux from the NCEP atmospheric reanalysis 2. The horizontal resolution of the GODAS data used here is $\frac{1}{3}^\circ$ latitude, 1° longitude.

A second reanalysis data set used here is the ECMWF Ocean Reanalysis System 4 (ORA-S4) [*Balmaseda et al*., 2013]. Monthly ocean temperature, salinity, and velocity fields from 1958 to 2014 are available on a resolution of 1° longitude and latitude, with meridional equatorial refinement to $\frac{1}{3}^\circ$, and 42 vertical levels. A 3DVAR configuration of NEMOVAR [*Daget et al*., 2009; *Mogensen et al*., 2012] is used to assimilate potential temperature, salinity, sea surface height, and the horizontal components of velocity.

Daily and monthly temperature time series of the Prediction and Research Moored Array in the Atlantic (PIRATA) are provided by the Tropical Atmosphere Ocean project (TAO) [*Servain et al*., 1998]. Observation periods and data gaps of the different buoys are listed in Table 1. The vertical resolution of temperature profiles is 20 m for the upper 140 m. There are additional temperature measurements at 180, 300, and 500 m depth.

Current velocity data along a 23°W section in the TA are acquired in the frame of the Tropical Atlantic Climate Experiment (TACE) [*Brandt et al*., 2014]. The horizontal velocity data were 40 h low-pass filtered and subsampled to 12 h intervals. By accounting for vertical instrument excursions, the velocity data were

Table 2. 2009 Depth Ranges and Temporal Data Gaps of TACE-Mooring Current Velocity Data Along 23°W

Latitude	Depth in m	Data Gaps
0.75°N	50–525	
0°N	35–625	
0.75°S	75–520	6–12 Nov 2009

interpolated on a vertical grid with a resolution of 10 m (mooring at 0°N, 23°W) or 5 m (moorings at ±0.75° N, 23°W). The depth range and data gaps of every mooring in the year 2009 are listed in Table 2.

Temperature and salinity profiles measured by Argo floats from 2005 to 2012 are used. Argo is a broad-scale global array of temperature and salinity profiling floats and is part of the integrated global observation strategy [*The Argo Science Team*, 2001]. Data Assembly Centers collect the data of Argo floats and apply a set of real time quality control tests. Only Argo float profiles with a quality flag of 1 (good data) within the TA (10°S–10°N) are used.

Anomalies of temperature, velocity, and SLA data as well as derived quantities from those data sets are calculated for the year 2009 by subtracting a monthly climatological seasonal cycle from the instantaneous data fields. The periods used for the climatological seasonal cycle are 1998–2011 for Tropical Rainfall Measuring Mission's (TRMM) Microwave Imager (TMI) SST and CCMP pseudo wind stress data, 2005–2012 for AVISO SLA and Argo Z_{20} data, 2006–2013 for PIRATA buoys data, and 1980–2014 for GODAS and ORA-S4 reanalysis data.

GODAS and ORA-S4 meridional velocity and temperature fields are used to calculate the Meridional Temperature Advection (MTA), $-v\frac{\partial T}{\partial y}$, by the prevailing meridional currents, where v is absolute meridional velocity in m s^{-1}, T is the temperature in °C, and y is latitude in m.

The depth of the 20°C-isotherm (Z_{20}) as a measure of thermocline depth is calculated from Argo float temperature profiles. Monthly mean Z_{20} maps of Argo data are constructed by linear interpolation of the data onto a 1°×1° grid using all data points available for a certain month.

Following the approach of *Hormann and Brandt* [2009], the propagation velocities of SLAs merdionally averaged within two latitude bands are estimated. The latitude bands are located at 3°N–6°N and 2°S–2°N between 40°W and 10°E. Reference SLA time series are calculated by averaging SLA between 26°W and 24°W in the respective latitude bands. We computed a lagged correlation of the SLA time series along a latitude band with its respective reference time series. The resulting correlation matrix depends on the time lag and longitude. We applied a least square fit to the lags of maximum correlation coefficients with respect to longitude. The linear slope of this fit is the wanted propagation velocity.

To describe the vertical structure of propagating waves in the EA in 2009, we apply an Empirical Orthogonal Function (EOF) analysis to isopycnal displacement profiles estimated from Argo float profiles. First, isopycnal displacement profiles are calculated with respect to a mean density profile in the TA in 2009 as follows: all Argo floats profiles in the TA in 2009 are selected in order to calculate potential density profiles. The profiles are then interpolated linearly onto a 5 m vertical resolution grid. To account for the density differences in the TA between the western and the eastern basin, three mean density profiles are calculated using only profiles measured between 40°W and 20°W, 20°W and 0°E, and 0°E and 10°E in 2009, respectively. For every single Argo float in the TA in 2009, an isopycnal displacement profile is then calculated with respect to the appropriate mean density profile. Linear interpolation is used to find the exact displacement. For the EOF analysis, profiles within two distinct latitude bands (2°S–2°N and 3°N–6°N) between 40°W and 10°E are selected. For each latitude band, the profiles (associated with latitude and time) are arranged as a two-dimensional matrix. The number of the profile is one dimension of the matrix and depth is the other one. We applied an EOF analysis to those matrices within a depth range of 20–300 m. The spatial pattern of the EOF analysis gives information about the vertical structure of the displacement profiles and the principle components show how they changed with time and longitude.

3. Results

First, the role of meridional advection of subsurface temperatures in the EA in boreal summer 2009 is analyzed. The results regarding the contribution of planetary waves in the 2009 cold event are presented in the second part of this section.

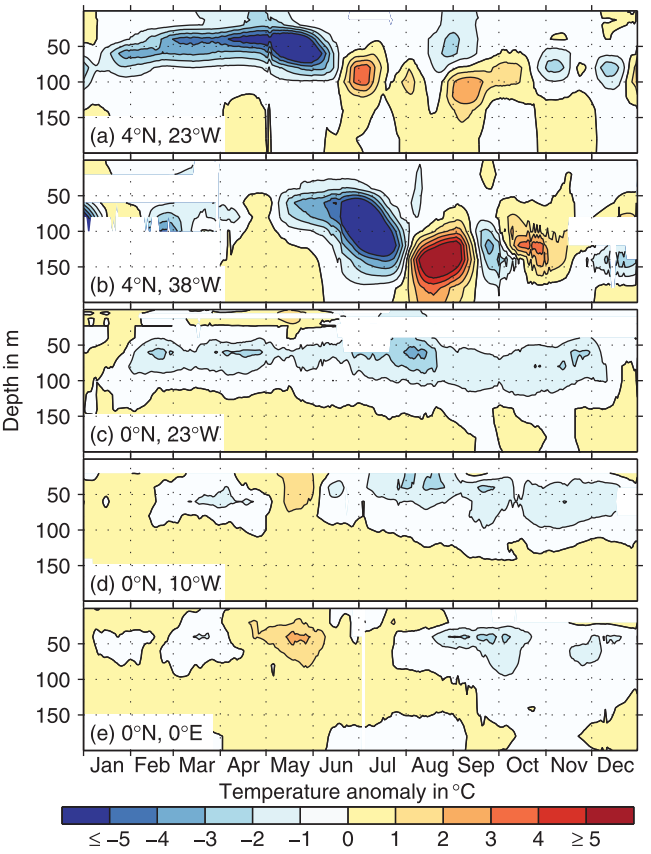

Figure 2. Time series of 2009 subsurface temperature anomalies with respect to the climatological mean (2006–2013) measured by PIRATA buoys at (a) 4°N, 23°W, (b) 4°N, 38°W, (c) 0°N, 23°W, (d) 0°N, 10°W, and (e) 0°N, 0°E. A 20 day running mean filter is applied to the daily data sets.

3.1. Meridional Advection

Richter et al. [2013] have suggested that direct meridional advection of subsurface temperature anomalies developing in boreal spring at about ~4°N can cause SST anomalies of the same sign in the ACT region in the following summer. The temperature anomalies are advected by the prevailing meridional subsurface currents that are commonly equatorward. In 2009, cold subsurface (upper 30–100 m) temperature anomalies are observed by PIRATA buoys at 4°N, 23°W during January–June and at 4°N, 38°W during May–July (Figure 2). The cold anomalies strengthen at 23°W during March–May and at 38°W during end of June–July. The cooling at 38°W extends down to a depth of 150 m. Both buoys show positive anomalies following the negative ones.

Compared to the anomalies along 4°N, the magnitude of the temperature anomalies along the equator are weaker (Figures 2c–2e). At 23°W, cold subsurface anomalies are present during end of January–mid-December. Positive temperature anomalies occur at the equatorial buoys at 10°W and 0°E during May and April–June, respectively. At 0°E, the positive anomalies extend to the surface. The positive anomalies at 10°W reach up to the shallowest measurement depth (30 m).

Subsurface temperature anomalies at 4°N can be advected toward the equator by the equatorward subsurface flow of the northern TC [*Richter et al.*, 2013]. TACE mooring observations at 23°W show southward subsurface meridional velocities with values between 3 and 6 cm s^{-1} at 0.75°N from February to August 2009 (Figure 3). At the Equator, southward velocities between 4 and 6 cm s^{-1} can be observed from March to April 2009 before they change flow direction every 1–2 months. At 0.75°S, velocities are southward in February–April, June–August as well as October–December and they are northward in January, May, and September.

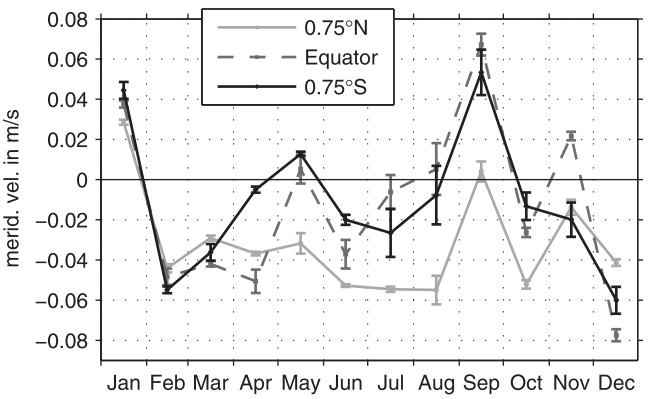

Figure 3. 2009 monthly means of meridional velocity from TACE mooring observations averaged (depending on the observational range) between 35 and 100 m at the equator (dark gray-dashed line), between 50 and 100 m at 0.75°N (gray solid line), and between 75 and 100 m at 0.75°S (black solid line).

The observed southward velocities at the equator and 0.75°N as well as the cold temperature anomalies at 4°N during the first half of 2009 suggest that meridional advection of subsurface temperature could have contributed to the anomalous cooling of SST along the equator. However, by using

the available moored velocity observations, it is not possible to unambiguously determine the strength of the TCs as the measurements are taken close to the equator in the transition zone between northern and southern TC.

To elucidate the meridional advection in more detail, we now focus on the quantification of the MTA in the EA in 2009. The available moored temperature and velocity measurements do not allow for a direct calculation of MTA, hence GODAS and ORA-S4 reanalysis data are used. Both data sets capture the observed SST and subsurface temperature anomalies in the TA in 2009 (see supporting information Figures S1 and S2).

Richter et al. [2013] analyzed advection terms averaged in the region 20°W–0°E, 3°S–3°N, 0–50 m and found the warming caused by meridional advection during noncanonical warm events to be most pronounced between 20 to 40 m depth. Their results show an increase in the meridional advection in the upper 50 m already in May, driving warm SST anomalies in the ACT region in June. For a noncanonical cold event, one would thus expect a cooling by MTA during May, prior to the occurrence of cold SST anomalies at the equator.

We customized the investigation area to the location where maximum cold temperature anomalies occur in the EA in 2009 (30°W–15°W, 3°S–3°N) and averaged the meridional advection term within different depth ranges down to 90 m depth, to account for the deeper extent of the TCs in the western Atlantic basin compared to the eastern Atlantic basin [*Perez et al*., 2014]. While there are differences between the anomalous MTA in 2009 from GODAS and ORA-S4, both data sets agree in that there is no anomalous cooling but rather warming by MTA in all depth ranges until May (Figure 4). After the onset of the cold event in June 2009, anomalous negative MTA can be observed in all depth ranges, which results in a strong cooling of the ACT region. From July onward, the anomalous MTA develops differently in the different depth ranges.

To better understand the MTA in the EA in 2009, we look at the temporal evolution of the temperature and velocity fields (Figure 5). In theory, the MTA is inversely proportional to the meridional temperature gradient ($\frac{dT}{dy}$) and the meridional velocity (v). Considering that the y axis is positive toward the North, cold subsurface temperatures anomalies at 4°N result in a negative $\frac{dT}{dy}$ toward the equator. As the prevailing subsurface currents between 0° and 4°N are commonly equatorward, v would be negative. Therefore, the resulting MTA is also negative and would lead to a cooling at the equator. During boreal spring 2009, cold subsurface temperature anomalies develop in the northern EA (Figures 5a, 5b, 5e, and 5f). Despite these cold temperature anomalies, the MTA is positive in boreal spring 2009. Until May 2009, the meridional velocities are weak compared to the following months. North of 2°N, poleward velocities reach down to over 100 m depth. The equatorward flow of the subsurface branch of the northern TC occurs south of 2°N. Note that the upper limb of the northern TC in the GODAS data extends up to 20 m deeper compared to the ORA-S4 data. This can be one reason for the difference in MTA values between the two data sets (Figure 4). Both the GODAS and the ORA-S4 meridional velocity fields indicate a weak northern TC in boreal spring 2009. A weakening of the TC is consistent with the results of *Foltz et al*. [2012]. They observed weaker upwelling just south of the equator due to the interannual north-westerly wind anomalies from January to April 2009.

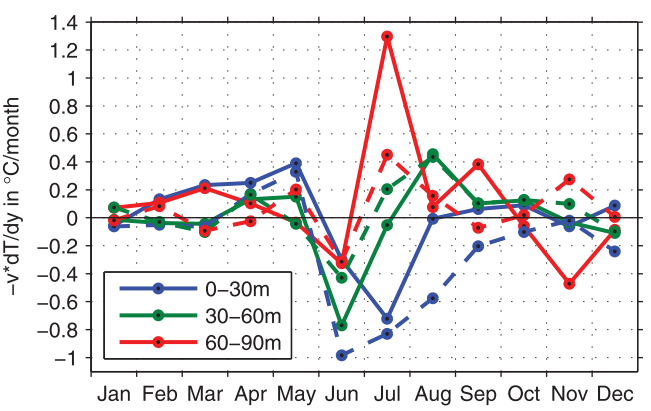

Figure 4. 2009 monthly means of anomalous MTA estimated from GODAS (solid) and ORA-S4 (dashed) temperature and velocity fields with respect to the climatology (1980–2014) within 30°W–15°W to 3°S–3°N for three different depth ranges (0–30 m in blue, 30–60 m in green, 60–90 m in red). Note that positive values indicate a warming and negative values indicate a cooling by meridional advection.

To determine the relative importance of the meridional velocity and temperature in the anomalous MTA, we have calculated the contribution of (i) the meridional advection of the anomalous temperature gradients in 2009 by the climatological currents, (ii) the meridional advection of the climatological temperature gradient by the anomalous meridional velocities in 2009, and (iii) the meridional advection of anomalous temperature gradient by the anomalous meridional velocities in 2009 (see supporting information Figure S3). In case (i), a comparatively

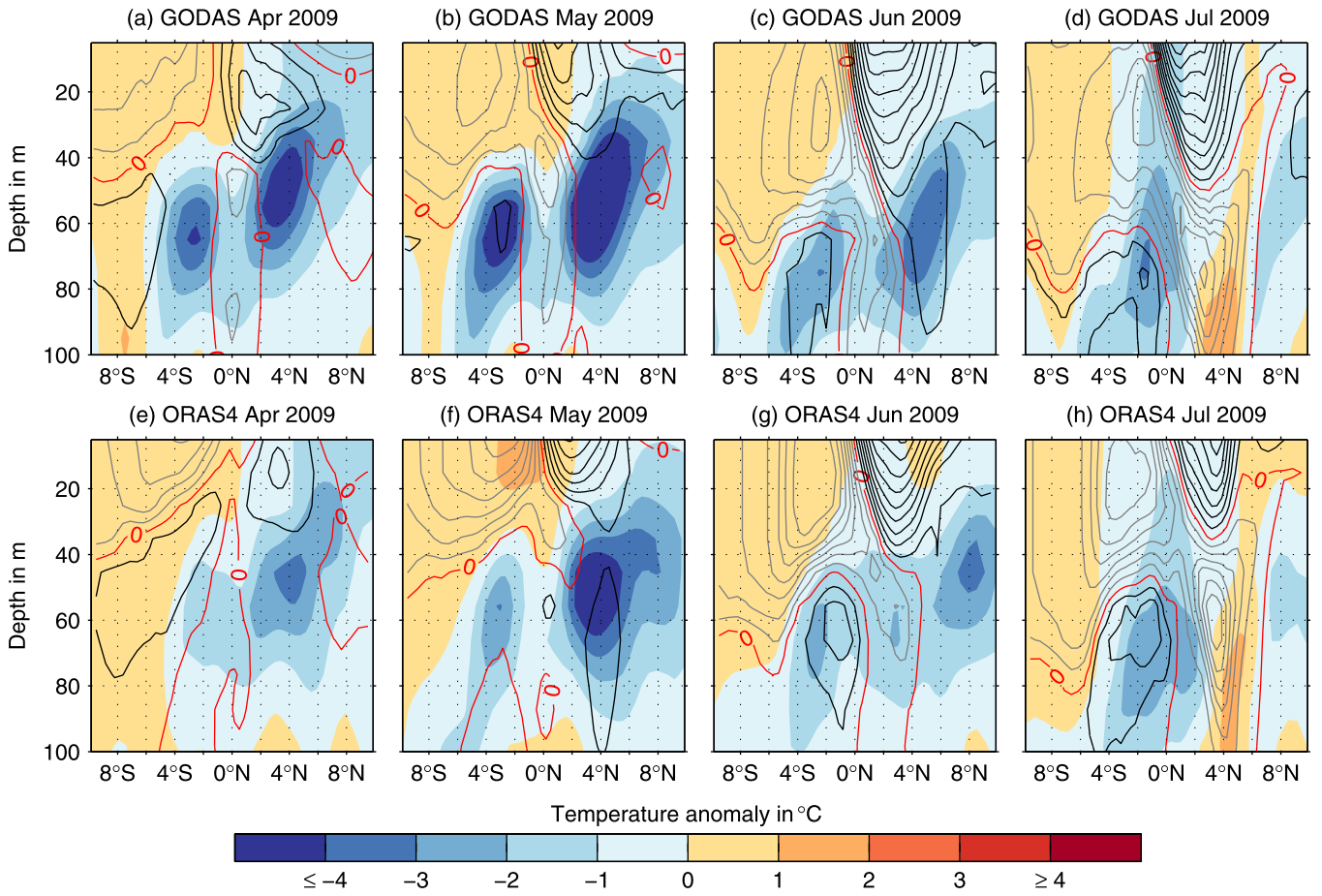

Figure 5. Latitude-depth section of monthly mean (top) GODAS and (bottom) ORA-S4 temperature anomalies (shading) with respect to the climatological mean (1980–2014) and total meridional currents (contours; interval 0.02 ms^{-1}, black lines indicate northward flow and gray lines southward flow, zero flow is marked by a red solid line) in 2009, averaged from 30°W to 15°W.

weak cooling by meridional advection can already be observed in April in GODAS data and in May in ORA-S4 data while there is a warming from July on. In case (ii), the monthly evolution of the MTA resembles that of the anomalous MTA in 2009, indicating that the meridional velocity sets the strength of the MTA. In case (iii), both data sets show a warming by meridional advection in the subsurface (30–60 m) between April and June.

To summarize, a cooling of the ACT region by MTA cannot be observed until June coinciding with the onset of the 2009 cold event. Note that the mechanism described by *Richter et al.* [2013] relies on the advection of subsurface temperature anomalies at 4°N by the mean meridional subsurface currents. The latter are dominated by the lower limb of the northern TC and are commonly equatorward [e.g., *McCreary and Lu*, 1994; *Molinari et al.*, 2003; *Perez et al.*, 2014]. However, in May 2009, the lower limb of the TC was too weak and located too far south to advect the cold subsurface temperature anomalies at 4°N toward the ACT region. Associated with the development of the ACT in June, the meridional velocities strengthened and extended further north again. Afterward, an advection of the cold subsurface temperature anomalies toward the equator was possible. This probably enhanced the cooling in the ACT region in boreal summer 2009, but it is unlikely that the abrupt cooling of SSTs along the equator is caused by meridional advection of subsurface temperatures. We will therefore investigate the second hypothesis, following *Foltz and McPhaden* [2010a] that the 2009 cold event was caused by upwelling equatorial waves.

3.2. Wave Reflection

Consistent with *Foltz and McPhaden* [2010a], indications for upwelling Rossby and reflected equatorial Kelvin waves can be found in the AVISO SLA data for 2009 (Figures 6a and 6b). Within the 3°N–6°N band (Figure 6a), negative SLAs develop in boreal spring, intensify in the central basin (~23° W) during April and

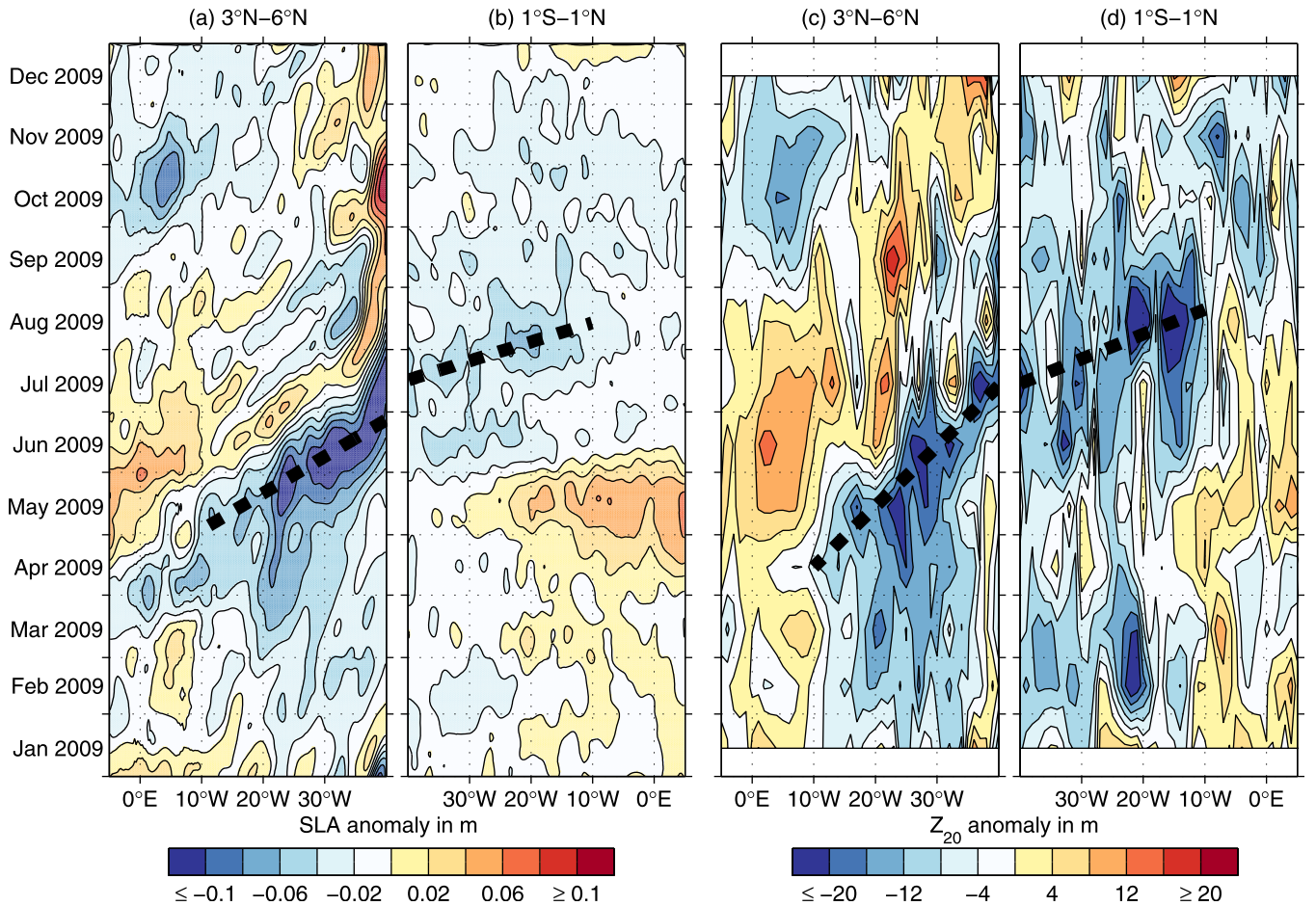

Figure 6. Anomalies of (a, b) AVISO SLA and (c, d) gridded Argo Z_{20} for the year 2009 with respect to the climatological mean (2005–2012), averaged in the latitude bands (a, c) 3°N–6°N and (b, d) 1°S–1°N. The daily SLA data were smoothed by a 20 day running mean filter. Monthly means of Argo Z_{20} data were linearly interpolated onto a 1° horizontal resolution grid. The black-dashed lines represent estimated propagation velocities of the negative anomalies of (a) -0.70 ms^{-1}, (b) 1.36 ms^{-1}, (c) 0.43 ms^{-1}, and (d) 1.05 ms^{-1}.

May, propagate westward and reach the western boundary during June–July. The estimated propagation velocity of the westward propagating negative anomalies is ∼0.70 m s^{-1} (see dashed line in Figure 6a). This value lies between the theoretical propagation speeds of first (∼0.80 m s^{-1}) and second (∼0.46 m s^{-1}) baroclinic mode Rossby wave, which is in agreement with the results of *Foltz and McPhaden* [2010a]. They described the westward propagating negative SLA as a pack of equatorial Rossby waves, forced by the north-westerly wind anomalies in the EA in 2009 (Figure 1).

Along the equator, an anomalous increase of SLAs during April and May 2009 (Figure 6b) is associated with warm SSTs and north-westerly wind anomalies (Figure 1). Eastward propagating negative SLAs develop at the western boundary from June to July when the pack of wind-induced Rossby waves described above reaches the western boundary. The negative SLAs signal propagates eastward and arrives at 10°W during June–September. The estimated propagation velocity of 1.36 m s^{-1} (see dashed line in Figure 6b) matches the one of a second baroclinic mode Kelvin wave (1.40 m s^{-1}) [*Illig et al.*, 2004; *Hormann and Brandt*, 2009]. It is curious that *Foltz and McPhaden* [2010a] find a lower propagation velocity of only ∼0.8 m s^{-1}. This discrepancy is most likely an expression of the high uncertainty that is associated with the estimation of velocities of propagating signals in observational data.

The magnitude of the negative SLAs along the equator is smaller by a factor of 2 compared to the respective signals along the 3°N–6°N band, suggesting a low reflection efficiency of baroclinic mode waves that are particularly visible in the SLA data.

Upwelling Rossby and Kelvin waves are not only associated with a depression in sea level but an uplifting of the thermocline. The depth of the 20°C isotherm (Z_{20}) from Argo data is used here as a measure of

thermocline depth. Consistent with the SLAs, negative Z_{20} anomalies (i.e., shallower than normal) propagate westward within the 3°N–6°N band during April–July (Figure 6c). Compared to the propagation velocity of the negative SLAs (black-dashed line in Figures 6a and 6c), the one of the negative Z_{20} anomalies appears to be slower. Maximum negative anomalies in the Z_{20} data occur earlier in the central Atlantic basin within the 3°N–6°N band and arrive later at the western boundary than the maximum negative anomalies in the SLA data.

Along the equator, a shallowing of the thermocline can be observed west of 10°W throughout the year 2009 (Figure 6d) despite the fact that strong positive SST anomalies and SLAs are present during April and May 2009. The anomalously shallow thermocline in the western/central EA coincides with the anomalously cold subsurface temperatures observed by PIRATA buoys (Figure 2c). East of 10°W a deepening of the thermocline is associated with warm subsurface temperature anomalies in the PIRATA data during May (Figures 2d and 2e). They are likely caused by downwelling, eastward propagating equatorial Kelvin waves, that are forced by the prevailing westerly wind anomalies in the central EA during boreal spring [*Foltz and McPhaden*, 2010a; *Lübbecke and McPhaden*, 2012].

Maximum negative Z_{20} anomalies occur in the western basin during June–August. They propagate eastward and reach 10°W during July–September. In contrast to the SLA, the westward propagating negative Z_{20} anomalies along the 3°N–6°N band and the eastward propagating ones along the equator have comparable magnitudes. The upwelling Kelvin wave signal that is visible in the Z_{20} data does not propagate further east than 10°W, possibly due to the 20°C-isotherm being located too shallow and close to the mixed layer in the eastern EA. An alternative explanation for the observed signal propagation of SLAs and Z_{20} anomalies may be the superposition of upwelling reflected Kelvin waves and downwelling reflected Rossby waves from the eastern boundary caused by wind-forced downwelling Kelvin waves in April and May 2009 [*Foltz and McPhaden*, 2010a].

The velocities of the westward propagating as well as the eastward propagating negative Z_{20} anomalies appear to be slower compared to the SLA data. In order to test whether this might be due to the sparse temporal and spatial data coverage of the Argo floats, Z_{20} data derived from the daily temperature data measured by PIRATA buoys are used for additional information. The propagation velocity of the maximum negative Z_{20} anomaly from the PIRATA buoy at 23°W, 4°N to the one at 38°W, 4°N is 0.43 m s^{-1} (black dashed line in Figure 6c). The propagation velocity of the maximum negative Z_{20} anomaly from the PIRATA buoy at 23°W, 0°N to the one at 10°W, 0°N is 1.05 m s^{-1} (black-dashed line in Figures 6a and 6d). Since these estimates are based on only two point measurements, they are afflicted with a high uncertainty. They do, however, match the peaks of the negative Z_{20} anomalies derived from Argo very well (Figures 6c and 6d) and thus confirm the slower propagation velocities compared to the SLAs.

The slower propagation velocity of the Z_{20} signal compared to the SLA signal and the fact that the amplitude of the thermocline anomalies along the equator is much higher than the amplitude of the corresponding sea level anomalies relative to the corresponding amplitudes along the 3°N–6°N band (Figures 6b and 6d) suggest that dynamics of baroclinic mode three and higher may be important for the development of the cold SST anomalies in the ACT region. We draw this conclusion because lower baroclinic mode waves travel faster and would have a stronger signature in SLA compared to higher baroclinic mode waves. *Illig et al*. [2004] have already pointed out the importance of higher baroclinic modes for SLA variability in the EA and the necessity to regard the variability in the vertical structure. Here, an EOF analysis is applied to isopycnal displacement profiles estimated from Argo floats to investigate the vertical structure of the observed propagating signals in the EA in 2009.

The EOF analysis is applied to isopycnal displacement profiles in two separate latitude bands (2°S–2°N and 3°N–6°N) between 40°W and 10°E. As mentioned in the methods section the EOF spatial pattern gives information about the vertical structure of the displacement profiles and the EOF principle components show how they changed with time and longitude (Figure 7). The vertical structure functions of the first EOF for both regions have their maximum within the thermocline. The explained variance of the first EOF is 52% in the northern region and 38% along the equator. Regarding the amplitudes of the first EOF at 3°N–6°N, a westward propagating signal with maximum negative amplitude can be found west of 20°W, reaching the western boundary between May and July. At 2°S–2°N, a negative signal propagates eastward from the western boundary as far as 5°E between May and September. This is in good agreement with the previous results, even though the eastward propagating signal is reaching further east in the EOF analysis of isopycnal displacements (Figure 7) than in the SLA and Z_{20} data (Figure 6).

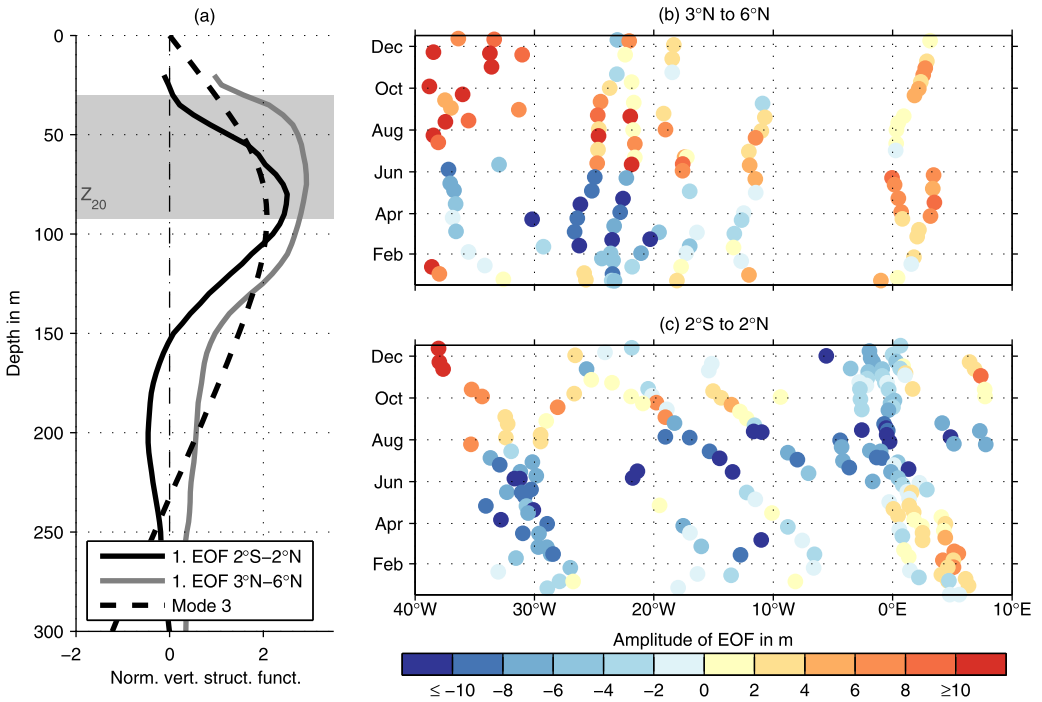

Figure 7. EOF analysis of density displacement profiles estimated from Argo floats profiles in the EA in 2009. (a) The black solid line shows the vertical structure function of the first EOF (explained variance is 38 %) derived from density displacement profiles within the latitude band 2°S to 2°N between 40°W and 10°E. The profiles are normalized by their standard deviation. The gray solid line shows the normalized vertical structure function of the first EOF (explained variance is 52 %) derived from density displacement profiles within the latitude band 3°N–6°N between 40°W and 10°E. The black-dashed line indicates the normalized vertical structure function of baroclinic mode three estimated from CTD profiles. The gray-shaded area marks the mean depth of the 20°C-isotherm ± its first standard deviation within the region 2°S–6°N, 40°W–10°E in 2009. Also shown are the amplitudes of the first EOF within (b) the northern and (c) the equatorial latitude band.

We now compare the vertical structure functions from the EOF analysis in both regions with those from a vertical mode decomposition. In general, the EOF vertical structure functions fit well to the vertical structure function of the third baroclinic mode, but they differ in one important characteristic. The vertical structure function of the 3°N–6°N region has no zero crossing in the upper 300 m, while the one of the equatorial region does have one at 150 m. In general, the higher the order of the baroclinic mode the shallower is the first zero crossing. Only the vertical structure functions of baroclinic mode one and two have no zero crossing within the upper 300 m. This suggests that the northern region is dominated by those two modes. The vertical structure function of baroclinic mode three has a zero crossing at ∼230 m, which is still deeper than the zero crossing of the vertical structure function in the equatorial region. This suggests that the equatorial region is influence by waves of baroclinic mode three and higher.

To further support this suggestion, we calculate the sea level displacement, that results from the observed vertical structure of isopycnal displacement. We integrate the ratio $\frac{\Delta\rho(z)}{\rho_0(z)}$ over the depth z (20–300 m), where ρ_0 is the mean density profile, $\Delta\rho$ is the difference between the displaced density profile and ρ_0. The maximum observed displacement in the northern latitude band, which is mainly associated with baroclinic mode 1–3 waves, results in a negative SLA of ∼0.18 m. The maximum observed displacement in the equatorial latitude band, which is mainly associated with waves of baroclinic mode three and higher, is ∼0.08 m. Although the vertical structure functions of both regions show a displacement of the thermocline of comparable magnitude, the resulting displacement of the sea surface differs notably. The observed values fit well with the maximum values of negative SLA in the AVISO data (Figure 6) supporting the hypothesis that also waves of baroclinic mode three and higher contribute to the cooling event in the ACT region in 2009.

Our analysis thus corroborates the results of *Foltz and McPhaden* [2010a] that the propagation of Rossby and Kelvin waves played an important role in the development of the 2009 cold event and in addition suggests that waves of baroclinic mode three and higher were involved.

4. Summary and Discussion

In 2009, a strong negative AMM event associated with north-westerly wind anomalies along the equator peaking in May was followed by a strong cold eastern equatorial Atlantic event that was most pronounced in August. The temperature drop from May to August 2009 and the ATL3 SSTs in August 2009 are the strongest and coldest on record, respectively [*Foltz and McPhaden*, 2010a; *Brandt et al*., 2014].

In the literature, two mechanisms have been discussed that provide possible explanations for the observed cold event in the TA in 2009. *Foltz and McPhaden* [2010a] suggested that upwelling equatorial Kelvin waves that were generated by the reflection of Rossby waves caused the cold event in 2009. *Richter et al*. [2013] on the other hand did not find that planetary waves are a main driver in the development of noncanonical warm events. They proposed instead that direct meridional advection can trigger noncanonical events as the one in the EA in 2009.

The results of this study suggest that a cooling by meridional advection took place during June and July but the analysis indicates that this mechanism is not of major importance for the onset of the 2009 cold event. On the other hand, the results confirm previous findings by *Foltz and McPhaden* [2010a] that planetary wave reflection processes causes the strong cooling in the EA in 2009.

Richter et al. [2013] and *Perez et al*. [2014] suggested that anomalous meridional advection of subsurface temperature anomalies can drive the development of the anomalous ACT events. Although strong negative subsurface temperature anomalies occur in the EA from February to May 2009 reaching as far south as 7°S, a cooling of the upper 90 m by meridional advection cannot be observed until June when the equatorward subsurface flow of the TCs is strengthening due to its seasonal cycle [*Perez et al*., 2014]. During boreal spring 2009, the usually equatorward subsurface meridional currents just north of the equator are weak or even slightly poleward in the region of maximum temperature anomalies. This is associated with the prevailing north-westerly wind anomalies that tend to weaken the northern TC which dominates the meridional flow pattern in the EA [*Molinari et al*., 2003; *Perez et al*., 2014]. A weakening of the TC in the first half of 2009 is also consistent with the results of *Foltz et al*. [2012]. They observed weaker than normal upwelling in the divergence zone of the TCs just south of the equator.

The results of this study thus suggest that meridional advection is of different importance for the onset of noncanonical warm and noncanonical cold events. During a noncanonical warm event, a positive AMM event develops in boreal spring [*Richter et al*., 2013]. The negative wind stress curl that is associated with a positive AMM event drives downwelling just north of the equator [*Foltz and McPhaden*, 2010b; *Lübbecke and McPhaden*, 2012; *Richter et al*., 2013] which leads to the development of warm subsurface temperature anomalies there. Stronger south-easterly winds on the equator in the western to central equatorial Atlantic act to strengthen the northern TC. The strengthened lower limb of the northern TC in turn advects the warm subsurface temperature anomalies toward the equator and warm the ACT region in boreal summer [*Richter et al*., 2013]. In contrast, associated with a negative AMM event during a noncanonical cold event, a positive wind stress curl anomaly during boreal spring leads to anomalous upwelling just north of the equator [*Foltz et al*., 2012]. As shown here, the northern TC weakens or even reverses the flow pattern associated with the north-westerly wind anomaly in the western to central equatorial Atlantic. Hence, there is no significant meridional advection of subsurface temperature that can drive an anomalous cooling of the ACT region in boreal summer. This asymmetry in the contribution of meridional advection to noncanonical warm and cold events may also explain why *Richter et al*. [2013] found more noncanonical warm than cold events.

Consistent with *Foltz and McPhaden* [2010a], signals of upwelling westward propagating Rossby waves and reflected eastward propagating equatorial Kelvin waves are observed in AVISO SLA and Z_{20} data derived from Argo float data. Analyzing in situ subsurface data by the means of vertical structure functions derived from an EOF analysis, we could show that the structure function fit well with that of a third baroclinic mode and that the main signal is propagating along the thermocline. Additionally, the vertical structure function associated with the Rossby waves appears to be influenced by baroclinic waves mode one and two. On the other hand, the vertical structure function associated with the Kelvin waves appears to be dominated by baroclinic mode waves even higher than mode three. *Illig et al*. [2004] investigated the contribution of long equatorial waves to the TA SLA variability and emphasized the importance of higher baroclinic mode waves. While the second baroclinic mode dominates, they found that the summed-up contribution of the fourth to

the sixth baroclinic mode to the TA SLA variability is as strong as the contribution of the two gravest modes. In this study, the propagation velocities of the forced Rossby and reflected Kelvin waves in the Z_{20} data are estimated to be smaller compared to that of the forced Rossby and reflected Kelvin waves in the SLA data. This supports our suggestion that higher baroclinic modes contributes to the variability in the vertical density and temperature structure at the equator. It has to be mentioned that the velocity estimates of the propagation signals in the observational data are afflicted with a high uncertainty. Regarding the amplitude, we observed a difference between the SLA and Z_{20} anomalies associated with the reflected Kelvin wave signal. Consistent with *Foltz and McPhaden* [2010a], the reflected equatorial Kelvin wave signal in the SLA data is small compared to the Rossby wave signal just north of the equator. In the Z_{20} data however, the forced Rossby and reflected Kelvin wave signals are of comparable magnitude. In combination with the results from the EOF analysis, this may suggest a weak reflection efficiency of low baroclinic mode waves and a relative enhancement of reflected higher baroclinic mode waves. In general, the SLAs associated with higher baroclinic mode waves are small compared to SLAs associated with low baroclinic mode waves, as shown here by estimating the SLAs which result from the vertical displacement profiles of the EOF analysis.

In summary, our results suggest that the 2009 cold event in the central EA basin developed as follows: in boreal spring 2009, the north-westerly wind anomalies in the EA drove anomalous upwelling between the equator and 6°N, west of 20°W [*Foltz et al*., 2012], and an anomalously weak EUC [*Brandt et al*., 2014; *Johns et al*.,]. Associated with the anomalous upwelling are cold subsurface temperature anomalies and an anomalous shoaling of the thermocline. This signal propagates westward north of the equator as Rossby waves and is partly reflected into equatorial Kelvin waves. In June 2009, the upwelling equatorial Kelvin waves arrive in the central EA basin and lead to an abrupt cooling of SST defining the onset of the ACT while the EUC stayed weak until July [*Brandt et al*., 2014]. Note, that subsurface temperature anomalies along the equator existed already since February, which favors the abrupt cooling of SST by upwelling equatorial waves. The cooling in June is enhanced by meridional advection of subsurface temperatures between 30°W and 15°W, thereby contributing to the development of the extreme cold SSTs in the eastern EA in August 2009.

Acknowledgments

This study was supported by the Deutsche Forschungsgemeinschaft as part of the Sonderforschungsbereich 754" Climate—Biogeochemistry Interactions in the Tropical Ocean," by the German Federal Ministry of Education and Research as part of the cooperative project RACE (03F0605B), SACUS (03G0837A), and by European Union 7th Framework Programme (FP7 20072013) under grant agreement 603521 PREFACE project. The altimeter data were produced by SSALTO/DUACS and distributed by AVISO with support from CNES (http://www.aviso.altimetry.fr/duacs/). TMI data are produced by Remote Sensing Systems and sponsored by the NASA Earth Sciences Program. Data are available at www.remss.com. GODAS data are provided by the NOAA/OAR/ESRL PSD, Boulder, Colorado, USA, on their website http://www.esrl.noaa.gov/psd/. The ECMWF ORA-S4 reanalysis data were obtained from ICDC (ftp://ftp.icdc.zmaw.de/EASYInit/ORA-S4/). With regard to the PIRATA data, we acknowledge the effort of the TAO project office of NOAA/PMEL (http://www.pmel.noaa.gov/pirata/). The Argo data were collected and made freely available by the International Argo Project and the national programs that contribute to it (http://www.Argo.ucsd.edu, http://Argo.jcommops.org). The Argo Program is part of the Global Ocean Observing System. Mooring velocity data are provided by the TACE observations working group on their website http://tace.geomar.de/index.html.

References

Atlas, R., R. N. Hoffman, J. Ardizzone, S. M. Leidner, J. C. Jusem, D. K. Smith, and D. Gombos (2011), A cross-calibrated, multiplatform ocean surface wind velocity product for meteorological and oceanographic applications, *Bull. Am. Meteor. Soc.*, *92*(2), 157–174, doi:10.1175/2010BAMS2946.1.

Balmaseda, M. A., K. Mogensen, and A. T. Weaver (2013), Evaluation of the ECMWF ocean reanalysis system ORA-S4, *Q. J. R. Meteorol. Soc.*, *139*(674), 1132–1161, doi:10.1002/qj.2063.

Behringer, D., and Y. Xue (2004), Evaluation of the global ocean data assimilation system at NCEP: The Pacific Ocean, in *Eighth Symposium on Integrated Observing and Assimilation Systems for Atmosphere, Oceans, and Land Surface*, *Am. Meteor. Soc.*, Seattle, Washington, 11–15 Jan.

Brandt, P., A. Funk, A. Tantet, W. E. Johns, and J. Fischer (2014), The Equatorial Undercurrent in the central Atlantic and its relation to tropical Atlantic variability, *Clim. Dyn.*, *43*, 1–13, doi:10.1007/s00382-014-2061-4.

Carton, J. A., X. Cao, B. S. Giese, and A. M. Da Silva (1996), Decadal and interannual SST variability in the tropical Atlantic Ocean, *J. Phys. Oceanogr.*, *26*(7), 1165–1175, doi:10.1175/1520-0485(1996)026 < 1165:DAISVI>2.0.CO;2.

Chang, P., L. Ji, and H. Li (1997), A decadal climate variation in the tropical Atlantic Ocean from thermodynamic air-sea interactions, *Nature*, *385*(6616), 516–518, doi:10.1038/385516a0.

Daget, N., A. Weaver, and M. Balmaseda (2009), Ensemble estimation of background-error variances in a three-dimensional variational data assimilation system for the global ocean, *Q. J. R. Meteorol. Soc.*, *135*(641), 1071–1094, doi:10.1002/qj.412.

Derber, J., and A. Rosati (1989), A global oceanic data assimilation system, *J. Phys. Oceanogr.*, *19*, 1333–1347, doi:10.1175/1520-0485(1989)019 < 1333:AGODAS>2. 0.CO;2.

Dibarboure, G., M.-I. Pujol, F. Briol, P. Y. L. Traon, G. Larnicol, N. Picot, F. Mertz, and M. Ablain (2011), Jason-2 in DUACS: Updated system description, first tandem results and impact on processing and products, *Mar. Geod.*, *34*, 214–241, doi:10.1080/01490419.2011.584826.

Foltz, G. R., and M. J. McPhaden (2010a), Abrupt equatorial wave-induced cooling of the Atlantic cold tongue in 2009, *Geophys. Res. Lett.*, *37*, L24605, doi:10.1029/2010GL045522.

Foltz, G. R., and M. J. McPhaden (2010b), Interaction between the Atlantic meridional and Niño modes, *Geophys. Res. Lett.*, *37*, L18604, doi:10.1029/2010GL044001.

Foltz, G. R., M. J. McPhaden, and R. Lumpkin (2012), A strong Atlantic meridional mode event in 2009: The role of mixed layer dynamics, *J. Clim.*, *25*, 363–380, doi:10.1175/JCLI-D-11-00150.1.

Hormann, V., and P. Brandt (2009), Upper equatorial Atlantic variability during 2002 and 2005 associated with equatorial Kelvin waves, *J. Geophys. Res.*, *114*, C03007, doi:10.1029/2008JC005101.

Illig, S., B. Dewitte, N. Ayoub, Y. Du Penhoat, G. Reverdin, P. De Mey, F. Bonjean, and G. S. E. Lagerloef (2004), Interannual long equatorial waves in the tropical Atlantic from a high-resolution ocean general circulation model experiment in 1981-2000, *J. Geophys. Res.*, *109*, C02022, doi:10.1029/2003JC001771.

Johns, W. E., P. Brandt, B. Bourlès, A. Tantet, A. Papapostolou, and A. Houk (2014), Zonal structure and seasonal variability of the Atlantic Equatorial Undercurrent, *Clim. Dyn.*, *43*, 3047–3069, doi:10.1007/s00382-014-2136-2.

Keenlyside, N. S., and M. Latif (2007), Understanding equatorial Atlantic interannual variability, *J. Clim.*, *20*, 131–142, doi:10.1175/JCLI3992.1.

Lu, P., J. P. McCreary, and B. A. Klinger (1998), Meridional circulation cells and the source waters of the Pacific equatorial undercurrent, *J. Phys. Oceanogr.*, *28*, 62–84, doi:10.1175/1520-0485(1998) 028 < 0062:MCCATS>2.0.CO;2.

Lübbecke, J. F., and M. J. McPhaden (2012), On the inconsistent relationship between Pacific and Atlantic Niños, *J. Clim.*, *25*, 4294–4303, doi:10.1175/JCLI-D-11-00553.1.

McCreary, J. P., and P. Lu (1994), Interaction between the subtropical and equatorial ocean circulations: The subtropical cell, *J. Phys. Oceanogr.*, *24*, 466–497 doi: 10.1175/1520-0485(1994)024 < 0466:IBTSAE>2.0.CO;2.

Mogensen, K., M. B. R. Molteni, and A. Weaver (2012), The NEMOVAR ocean data assimilation system as implemented in the ECMWF ocean analysis system for System 4, *ECMWF Tech. Mem.*, 668, Eur. Cent. for Medium-Range Weather Forecasts, Reading, England. [Available at at http://www.ecmwf.int/en/elibrary/11174-nemovar-ocean-data-assimilation-system-implemented-ecmwf-ocean-analysis-system-4.]

Molinari, R. L., S. Bauer, D. Snowden, G. C. Johnson, B. Bourles, Y. Gouriou, and H. Mercier (2003), A comparison of kinematic evidence for tropical cells in the Atlantic and Pacific Oceans, *Elsevier Oceanogr. Ser.*, *68*(C), 269–286, doi:10.1016/S0422-9894(03)80150-2.

Perez, R. C., V. Hormann, R. Lumpkin, P. Brandt, W. E. Johns, F. Hernandez, C. Schmid, and B. Bourlès (2014), Mean meridional currents in the central and eastern equatorial Atlantic, *Clim. Dyn.*, *43*, 2943–2962, doi:10.1007/s00382-013-1968-5.

Philander, S. G. H. (1986), Unusual conditions in the tropical Atlantic Ocean in 1984, *Nature*, *322*, 236–238, doi:10.1038/322236a0.

Richter, I., S. K. Behera, Y. Masumoto, B. Taguchi, H. Sasaki, and T. Yamagata (2013), Multiple causes of interannual sea surface temperature variability in the equatorial Atlantic Ocean, *Nat. Geosci.*, *6*(1), 43–47, doi:10.1038/ngeo1660.

Servain, J., A. J. Busalacchi, M. J. McPhaden, A. D. Moura, G. Reverdin, M. Vianna, and S. E. Zebiak (1998), A pilot research moored array in the tropical Atlantic (PIRATA), *Bull. Am. Meteor. Soc.*, *79*, 2019–2031, doi:10.1175/1520-0477(1998)079 < 2019:APRMAI>2.0.CO;2.

The Argo Science Team (2001), Argo: The global array of profiling floats, in *Observing the oceans in the 21st century*, edited by C. J. Koblinsky, and N. R. Smith, pp. 248–258, GODAE Proj. Off. and Bur. of Meteorol., Melbourne, Australia.

Zebiak, S. E. (1993), Air-sea interaction in the equatorial Atlantic region, *J. Clim.*, *6*(8), 1567–1586, doi:10.1175/1520-0442(1993)006 < 1567:AIITEA>2.0.CO;2.